Computers and Geosciences 123 (2019) 47–58

Contents lists available at ScienceDirect

Computers and Geosciences

journal homepage: www.elsevier.com/locate/cageo

IGiK–TVGMF: A MATLAB package for computing and analysing temporal variations of gravity/mass functionals from GRACE satellite based global geopotential models

Walyeldeen Godah[1]

Institute of Geodesy and Cartography, Centre of Geodesy and Geodynamics, 27 Jacka Kaczmarskiego St., 02-679 Warsaw, Poland

ARTICLE INFO

Keywords:
GGM
GRACE
Gravity/mass functionals
MATLAB
PCA/EOF
Seasonal adjustment

ABSTRACT

The determination and the analysis of temporal variations of gravity/mass functionals (TVGMFs) are one of the most important tasks within the Earth-science disciplines. This paper describes a MATLAB package, named IGiK–TVGMF (Instytut Geodezji i Kartografii–TVGMF). This MATLAB package allows computing and analysing TVGMF from Global Geopotential Models (GGMs) that developed on the basis of a monthly interval GRACE (Gravity Recovery And Climate Experiment) satellite gravimetry mission data.

The IGiK–TVGMF package is developed using the MATLAB App Designer. Thirteen TVGMFs from seven GRACE computation centres can be determined at a single point or a grid of points, using the IGiK–TVGMF. The seasonal adjustment and the Principal Component Analysis/Empirical Orthogonal Function (PCA/EOF) methods were utilized to analyse and model TVGMFs.

The IGiK–TVGMF is freely available for non-commercial, scientific research and academic purposes via https://github.com/Walyeldeen/Walyeldeen-Godah.

1. Introduction

The determination and the analysis of temporal mass variations within the Earth system are one of the main scientific objectives in the Earth science-related disciplines. The Gravity Recovery and Climate Experiment (GRACE, e.g. Tapley et al., 2004) satellite mission launched in March 2002 with its pioneering observation technology (satellite to satellite tracking in a low-low mode) provides valuable data for the determination of temporal variations of gravity/mass functionals (TVGMFs). The distance between twin satellites following each other in the same orbit is measured by K-band microwave ranging (KBR) instrument. The GRACE satellite mission was operated for three times longer than its initial planned duration. In October 2017, GRACE satellites ran out of fuel, and the mission was terminated. However, it emphasizes the need for the GRACE Follow-On (GRACE-FO) satellite mission, which has been launched on 22nd May 2018 (see https://gracefo.jpl.nasa.gov/), for a long-term sustainable information on TVGMFs. Besides GRACE satellite mission data, monthly Global Geopotential Models (GGMs) from kinematic orbits of low-Earth orbiting satellites, e.g. the CHAllenging Minisatellite Payload (CHAMP; Reigber et al., 2002) satellite mission (e.g. Weigelt et al., 2013) and non-dedicated gravity satellite missions (e.g. Jason, Kompsat, MetOp, Sentinel, SWARM, TanDEM-X, TerraSAR-X; https://www.tugraz.at/institute/ifg/projects/theoretical-geodesy-and-satellite-geodesy/tvgogo/), have also been developed and utilized for the determination of TVGMFs. However, the use of GRACE KBR data currently yields the best monthly GGMs, in terms of the accuracy and the spatial resolution of GGMs, compared to the corresponding ones developed with the use of kinematic orbits, i.e. satellite to satellite tracking in a high-low mode data (cf. Weigelt et al., 2013; Zehentner et al., 2014).

In order to determine and analyse TVGMFs using GGMs from GRACE mission data, an appropriate computational tool is essentially needed. In the last few decades, considerable contributions have been devoted to compute gravity/mass functionals from GGMs using different computer programing languages, e.g. FORTRAN (e.g. Rapp, 1982; Tscherning et al., 1983; Holmes and Pavlis, 2006), Python (e.g. Nielsen et al., 2012) and MATLAB (e.g. Kiamehr and Eshagh, 2008; Bucha and Janák, 2013). Moreover, several interactive online tools, e.g. the International Centre for Global Earth Models (ICGEM; Barthelmes, 2016; http://icgem.gfz-potsdam.de/home), the CU (Colorado University) GRACE Data Portal; (http://geoid.colorado.edu/grace/), the Australian National University GRACE visualization web portal (Darbeheshti et al., 2013; http://grace.anu.edu.au/evasph.php) and the European Gravity Service for Improved Emergence Management

E-mail address: walyeldeen.godah@igik.edu.pl.
[1] Walyeldeen Godah is the sole author on this paper.

https://doi.org/10.1016/j.cageo.2018.11.008
Received 3 April 2018; Received in revised form 2 November 2018; Accepted 15 November 2018
Available online 17 November 2018

(EGSIEM; http://plot.egsiem.eu/) have been developed for the computation of static GMFs and TVGMFs. The main limitations of currently available softwares and interactive online tools developed for the computation of static GMFs and TVGMFs can be ascribed as follows:

- The currently available softwares were mainly developed to determine static gravity functionals. Thus, in order to compute TVGMFs using these software, users may need to conduct a preprocessing or modify GRACE-based GGMs. For example, users may require to replace the second degree and order (d/o) spherical harmonic coefficient of GRACE-based GGMs for each month. Moreover, these softwares do not allow users to determine temporal variations of mass functionals, e.g. the equivalent water thickness, surface deformation and physical height changes, from GRACE-based GGMs. Furthermore, for some of these softwares, users may need to determine TVGMFs from GRACE-based GGMs month by month, which would be very time and manpower consuming.
- Interactive online tools cannot be used without Internet connection. Moreover, the computation time of TVGMFs using these interactive online tools depends on the quality, e.g. the stability, speed, etc., of the Internet. Additionally, available interactive online tools do not include an option for the determination of some TVGMFs, e.g. temporal variations of deflection of verticals, physical height changes and temporal variations of surface deformations.
- These softwares and interactive online tools do not allow users analyse and model TVGMFs.

Taking into the consideration these limitations, the main objective and motivation of this contribution are to develop a novel MATLAB package, named the IGiK–TVGMF (Instytut Geodezji i Kartografii–TVGMF), for the determination, analysis and modelling of TVGMFs. This MATLAB package allows users to compute and analyse thirteen types of TVGMFs at a single point or a grid of points using GRACE-based GGMs. The data and methods that are used to perform the computation, and the analysis of those TVGMFs are described. An overview discusses main features of the IGiK–TVGMF, is followed by examples of results and validations of TVGMFs using the IGiK–TVGMF.

2. Data used

Since the launch of GRACE satellite mission, GGMs developed on the basis of GRACE mission data of different time intervals, e.g. monthly, weekly and daily interval, are provided by several computational centres. In the IGiK–TVGMF, the focus is on the latest release of monthly GRACE-based GGMs from the GFZ (GeoForschungs Zentrum), the CSR (Centre for Space Research) and the JPL (Jet Propulsion Laboratory), the ITG (Institut für Geodäsie und Geoinformation of Bonn University), the AIUB (Astronomical Institute of Bern University), the HUST (Huazhong University of Science and Technology) and the Tongji (Tongji University). These GGMs were obtained from the ICGEM (http://icgem.gfz-potsdam.de/ICGEM/ICGEM.html). They are specified in Table 1. They are available as spherical harmonic coefficients, i.e. Stokes coefficients (fully normalised) $C^W_{\ell m}$ and $S^W_{\ell m}$, developed up to a certain d/o, ℓ and m, respectively.

Table 1
GRACE-based GGMs used in the IGiK–TVGMF.

Computation centres	Maximum d/o	Reference
AIUB Release 02	90	Meyer et al. (2016)
CSR Release 05	96	Bettadpur, 2013
GFZ Release 05	90	Dahle et al. (2014)
HUST-Grace2016	60	Zhou et al. (2017)
ITSG-Grace2016	120	Klinger et al. (2016)
JPL Release 05	60	Watkins and Yuan (2014)
Tongji Release 02	60	Chen et al. (2015)

In addition to monthly GRACE-based GGMs in the IGiK–TVGMF, load Love numbers are calculated using the Preliminary Reference Earth Model (PREM; Dziewonski and Anderson, 1981). The numerical values of load Love numbers were obtained from Wang et al. (2012). Also, the monthly second d/o spherical harmonic coefficient C_{20}, that represents changes in the Earth's dynamic oblateness, is estimated from GRACE, Ocean Bottom Pressure (GRACE-OBP) data with/without restoring the Glacial Isostatic Adjustment (GIA) signal (Sun et al., 2016) and satellite laser ranging (SLR) data (Cheng et al., 2013). In order to eliminate static components of gravity/mass functional (GMF), state-of-the-art combined GGMs, i.e. the EGM2008 (Earth Gravitational Model 2008; Pavlis et al., 2012), the EIGEN-6C4 (European Improved Gravity model of the Earth by New techniques; Förste et al., 2014), and the GECO (GOCE and EGM2008 COmbined model; Gilardoni et al., 2016), were used as reference models.

3. Methods

Two methods are implemented to develop the IGiK–TVGMF. The first one concerns the determination of the TVGMF, while the second one concerns the analysis and modelling of the TVGMF. In this section, these two methods are specified.

3.1. The determination of the TVGMF

The fundamental theory concerning the determination of gravity/mass functionals from spherical harmonic coefficients has widely been presented in the geodetic textbooks (e.g. Heiskanen and Moritz, 1967; Torge and Müller, 2012) as well as by many authors (e.g. Wahr et al., 1998; Kusche and Schrama, 2005). According to Barthelmes (2013), functionals of the geopotential, e.g. the stationary part of the Earth's gravitational potential W_a, the disturbing potential T, the geoid height N, the spherical approximation of gravity disturbance δg_{sa} and the spherical approximation of gravity anomaly Δg_{sa}, at any point on and above the Earth's surface, are expressed as follows:

$$W_{a(r,\lambda,\varphi)} = \frac{GM}{r}\sum_{\ell=0}^{\ell_{\max}}\sum_{m=0}^{\ell}\left(\frac{R}{r}\right)^{\ell} P_{\ell m}(\sin\varphi)(C^W_{\ell m}\cos m\lambda + S^W_{\ell m}\sin m\lambda) \tag{1}$$

$$T_{(r,\lambda,\varphi)} = \frac{GM}{r}\sum_{\ell=0}^{\ell_{\max}}\left(\frac{R}{r}\right)^{\ell}\sum_{m=0}^{\ell} P_{\ell m}(\sin\varphi)(C^T_{\ell m}\cos m\lambda + S^T_{\ell m}\sin m\lambda) \tag{2}$$

$$N_{(\lambda,\varphi)} = \frac{GM}{r_e\gamma(r_e,\varphi)}\sum_{\ell=0}^{\ell_{\max}}\left(\frac{R}{r_e}\right)^{\ell}\sum_{m=0}^{\ell} P_{\ell m}(\sin\varphi)(C^T_{\ell m}\cos m\lambda + S^T_{\ell m}\sin m\lambda) - N^T \tag{3a}$$

$$N^T = \frac{2\pi G\rho}{\gamma(r_e,\varphi)}\left[R\sum_{\ell=0}^{\ell_{\max}}\sum_{m=0}^{\ell} P_{\ell m}(\sin\varphi)(C^{topo}_{\ell m}\cos m\lambda + S^{topo}_{\ell m}\sin m\lambda)\right]^2 \tag{3b}$$

$$\delta g_{sa(r,\lambda,\varphi)} = \frac{GM}{r^2}\sum_{\ell=0}^{\ell_{\max}}\left(\frac{R}{r}\right)^{\ell}(\ell+1)\sum_{m=0}^{\ell} P_{\ell m}(\sin\varphi)(C^T_{\ell m}\cos m\lambda + S^T_{\ell m}\sin m\lambda) \tag{4}$$

$$\Delta g_{sa(r,\lambda,\varphi)} = \frac{GM}{r^2}\sum_{\ell=0}^{\ell_{\max}}\left(\frac{R}{r}\right)^{\ell}(\ell-1)\sum_{m=0}^{\ell} P_{\ell m}(\sin\varphi)(C^T_{\ell m}\cos m\lambda + S^T_{\ell m}\sin m\lambda) \tag{5}$$

with

$$C^T_{lm} = C^W_{lm} - C^U_{lm} \text{ and } S^T_{lm} = S^W_{lm} - S^U_{lm} \tag{6}$$

where r, φ, λ are spherical geocentric coordinates of the computation point, R is the reference radius, GM is the product of the Newtonian gravitational constant G and the Earth's mass M, $C^U_{\ell m}$ and $S^U_{\ell m}$ denote

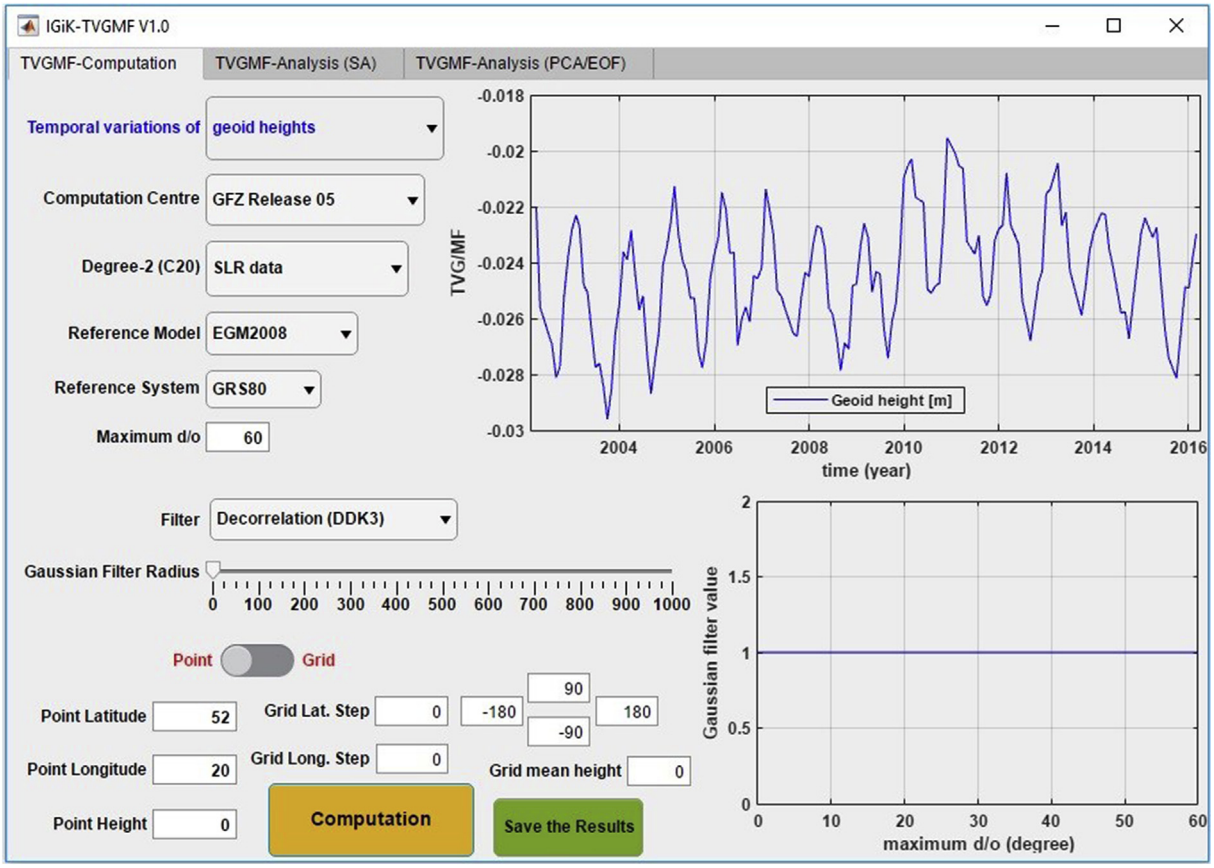

Fig. 1. Temporal variation of geoid heights at point P ($\varphi = 52^{\circ}$N, $\lambda = 20^{\circ}$E, $h = 0$) from the TVGMF–Computation.

spherical harmonic coefficients of the normal gravity field, $C_{\ell m}^{topo}$ and $S_{\ell m}^{topo}$ are dimensionless spherical harmonic coefficients of the topographic potential obtained on the basis of fully normalised spherical harmonic coefficients of the elevations (e.g. Pavlis et al., 2012; Eq. (33)) that determined from a global gridded topographic model, r_e is the geocentric radius of the computation point on the ellipsoid, γ denotes the normal gravity, ρ is the mass density and $P_{\ell m}$ are the fully normalised Legendre functions determined with the use of a recursive algorithm (cf. Appendix A). It should be mentioned that in Eq. (6), zonal coefficients of the spherical harmonic gravity model $C_{2\ell,0}^{U}$, $\ell = 1, 2, 3, 4$, were obtained by rescaling the corresponding ones $\widehat{C}_{2\ell,0}^{U}$ of the selected reference system, e.g. GRS80, WGS84, as follows (e.g. Barthelmes, 2013, p. 19, Eq. 111):

$$C_{2\ell,0}^{U} = \widehat{C}_{2\ell,0}^{U} \times \frac{GM^{U}}{GM^{GGM}} \left(\frac{R^{U}}{R^{GGM}} \right)^{\ell} \tag{7}$$

where GM^{U} and GM^{GGM} – geocentric gravitational constants of the reference system and the GGM, respectively. R^{U} and R^{GGM} – radii of the Earth of the reference system and the *GGM*, respectively. In the IG-iK–TVGM the interest is on TVGMF values instead of GMF values form GRACE-based GGMs with respect to reference model, e.g. the EGM2008, EIGEN-6C4, GECO. Thus, the differences $\Delta C_{\ell m}^{W}$, $\Delta C_{\ell m}^{W}$ and $\Delta C_{\ell m}^{T}$, $\Delta S_{\ell m}^{T}$ between spherical harmonic coefficients $C_{\ell m}^{W(\mathrm{GRACE})}$, $S_{\ell m}^{W(\mathrm{GRACE})}$ from GRACE-based GGMs and $C_{\ell m}^{W(\mathrm{Ref.\ mod.})}$, $S_{\ell m}^{W(\mathrm{Ref.\ mod.})}$ from a selected reference model are as follows:

$$\left.\begin{aligned}
\Delta C_{\ell m}^{W} &= C_{\ell m}^{W(\mathrm{GRACE})} - C_{\ell m}^{W(\mathrm{Ref.\ mod.})} \\
\Delta S_{\ell m}^{W} &= S_{\ell m}^{W(\mathrm{GRACE})} - C_{\ell m}^{W(\mathrm{Ref.\ mod.})} \\
\Delta C_{\ell m}^{T} &= C_{\ell m}^{W(\mathrm{GRACE})} - C_{\ell m}^{U(\mathrm{GRACE})} - (C_{\ell m}^{W(\mathrm{Ref.\ mod.})} - C_{\ell m}^{U(\mathrm{Ref.\ mod.})}) \\
\Delta S_{\ell m}^{T} &= S_{\ell m}^{W(\mathrm{GRACE})} - S_{\ell m}^{U(\mathrm{GRACE})} - (S_{\ell m}^{W(\mathrm{Ref.\ mod.})} - S_{\ell m}^{U(\mathrm{Ref.\ mod.})})
\end{aligned}\right\} \tag{8}$$

where $C_{\ell m}^{U(\mathrm{GRACE})}$, $S_{\ell m}^{U(\mathrm{GRACE})}$ and $C_{\ell m}^{U(\mathrm{Ref.\ mod.})}$, $S_{\ell m}^{U(\mathrm{Ref.\ mod.})}$ are rescaled (cf. Eq. (7)) spherical harmonic coefficients of the normal gravity field of GRACE-based GGMs and the reference GGM, respectively.

With the use of $\Delta C_{\ell m}^{T}$ and $\Delta S_{\ell m}^{T}$, temporal variations of gravity functionals (presented in Eqs. (1)–(5)) are determined in the IG-iK–TVGM as follows:

$$\Delta W_{a(r,\lambda,\varphi)} = \frac{GM}{r} \sum_{\ell=0}^{\ell_{\max}} \sum_{m=0}^{\ell} \left(\frac{R}{r} \right)^{\ell} P_{\ell m}(\sin\varphi)(\Delta C_{\ell m}^{W} \cos m\lambda + \Delta S_{\ell m}^{W} \sin m\lambda) \tag{9}$$

$$\Delta T_{(r,\lambda,\varphi)} = \frac{GM}{r} \sum_{\ell=0}^{\ell_{\max}} \left(\frac{R}{r} \right)^{\ell} \sum_{m=0}^{\ell} P_{\ell m}(\sin\varphi)(\Delta C_{\ell m}^{T} \cos m\lambda + \Delta S_{\ell m}^{T} \sin m\lambda) \tag{10}$$

$$\Delta N_{(\lambda,\varphi)} = \frac{GM}{r_e \gamma(r_e,\varphi)} \sum_{\ell=0}^{\ell_{\max}} \left(\frac{R}{r_e} \right)^{\ell} \sum_{m=0}^{\ell} P_{\ell m}(\sin\varphi)(\Delta C_{\ell m}^{T} \cos m\lambda + \Delta S_{\ell m}^{T} \sin m\lambda) \tag{11}$$

$$\Delta \delta g_{sa(r,\lambda,\varphi)} = \frac{GM}{r^2} \sum_{\ell=0}^{\ell_{\max}} \left(\frac{R}{r} \right)^{\ell} (\ell + 1) \sum_{m=0}^{\ell} P_{\ell m}(\sin\varphi)(\Delta C_{\ell m}^{T} \cos m\lambda + \Delta S_{\ell m}^{T} \sin m\lambda) \tag{12}$$

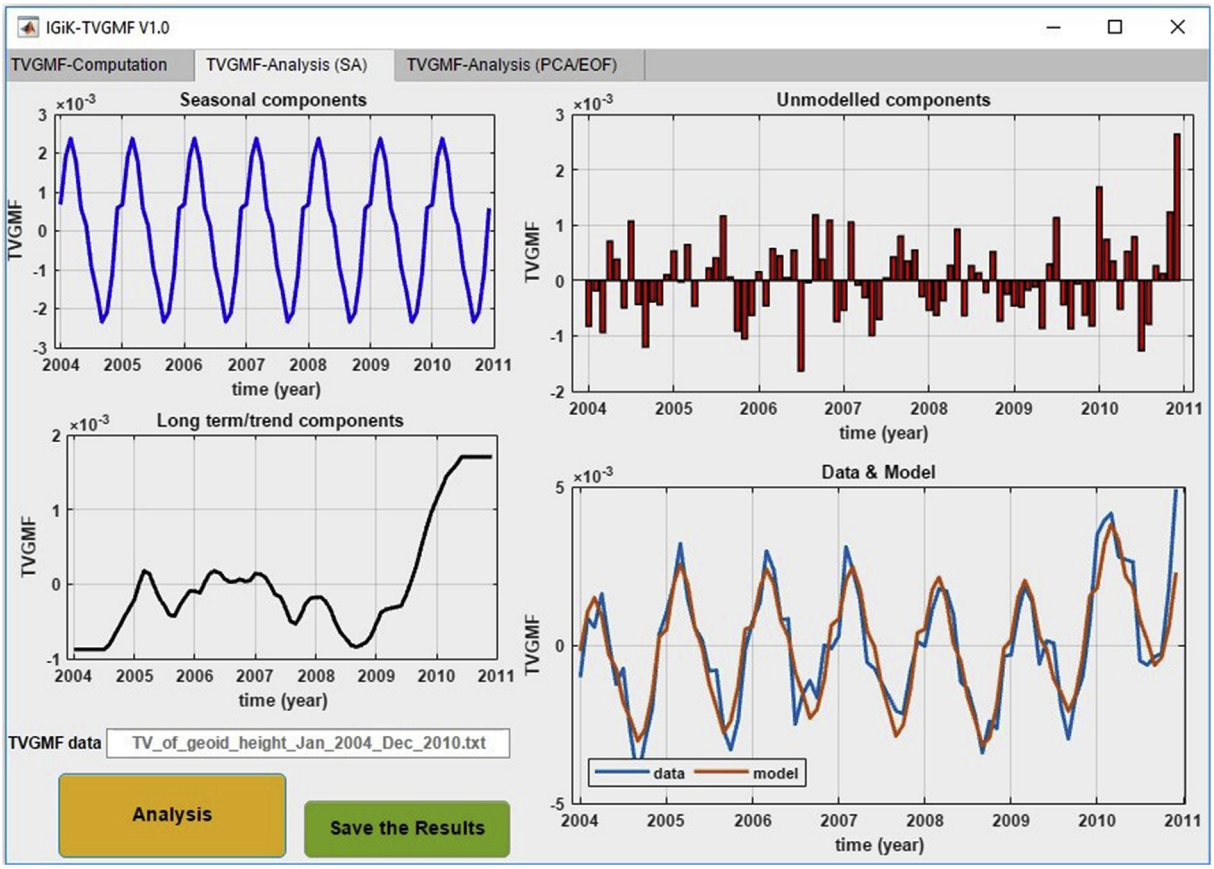

Fig. 2. Analysis of temporal variations of geoid heights at point P ($\varphi = 52^{\circ}$N, $\lambda = 20^{\circ}$E, $h = 0$) for the period between January 2004 and December 2010 using the TVGMF–Analysis (SA).

$$\Delta\Delta g_{sa(r,\lambda,\varphi)} = \frac{GM}{r^2}\sum_{\ell=0}^{\ell_{\max}}\left(\frac{R}{r}\right)^{\ell}(\ell-1)\sum_{m=0}^{\ell}P_{\ell m}(\sin\varphi)(\Delta C_{\ell m}^{T}\cos m\lambda + \Delta S_{\ell m}^{T}\sin m\lambda) \tag{13}$$

It should be noted that, in the IGiK–TVGMF, ΔN are determined instead of N. Thus, the contribution of geoid heights signal induced from the topography, i.e. the term N^{T} in Eq. (3a), is vanished completely. Moreover, the zero-degree term in gravity field parameters is also eliminated. This is because the Earth mass M, the mass of the ellipsoid M', the potential of the geoid W^{0} and the potential of the reference ellipsoid U^{0}, from the reference system, e.g. GRS80 or WGS84, applied to determine GMFs from GRACE-based GGMs are equal to the corresponding ones applied to determine GMFs from the reference model.

Moreover, temporal variations of gravity gradient (2nd vertical derivative) ΔT_{rr}, temporal variations of equivalent water thickness ΔEWT and temporal variations of deflection of the vertical in north–south $\Delta\xi$ and east–west $\Delta\eta$ components as well as temporal variations of surface deformation in the east Δe, north Δn and up Δh components are computed using $\Delta C_{\ell m}^{T}$ and$\Delta S_{\ell m}^{T}$. The mathematical formulae used to determine these TVGMFs are:

Temporal variations of gravity gradient (2nd vertical derivative) (Torge and Müller, 2012, p. 273, Eq. 6.138);

$$\Delta T_{rr(r,\varphi,\lambda)} = \frac{GM}{r^3}\sum_{\ell=2}^{\ell_{\max}}(\ell+1)(\ell+2)\left(\frac{a}{r}\right)^{\ell}\sum_{m=0}^{\ell}(\Delta C_{\ell m}^{T}\cos m\lambda + \Delta S_{\ell m}^{T}\sin m\lambda)P_{\ell m}(\sin\varphi) \tag{14}$$

Temporal variations of equivalent water thickness (Wahr et al., 1998);

$$\Delta EWT_{(r,\varphi,\lambda)} = \frac{a\times\rho_{ave}}{3}\sum_{\ell=0}^{\ell_{\max}}\sum_{m=0}^{\ell}P_{\ell m}(\sin\varphi)\frac{2\ell+1}{1+k_{\ell}}(\Delta C_{\ell m}^{T}\cos m\lambda + \Delta S_{\ell m}^{T}\sin m\lambda) \tag{15}$$

Temporal variations of deflection of the vertical in north–south and in east–west components (Torge and Müller, 2012, p. 273, Eqs. 6.137a and 6.137b);

$$\Delta\xi_{(r,\varphi,\lambda)} = \frac{GM}{r^2\gamma}\sum_{\ell=2}^{\ell_{\max}}\left(\frac{a}{r}\right)^{\ell}\sum_{m=0}^{\ell}(\Delta C_{\ell m}^{T}\cos m\lambda + \Delta S_{\ell m}^{T}\cos m\lambda)\frac{\partial P_{\ell m}(\sin\varphi)}{\partial\varphi} \tag{16}$$

$$\Delta\eta_{(r,\varphi,\lambda)} = \frac{GM}{r^2\gamma\cos\varphi}\sum_{\ell=2}^{\ell_{\max}}\left(\frac{a}{r}\right)^{\ell}\sum_{m=0}^{\ell}(-m\Delta C_{\ell m}^{T}\sin m\lambda + m\Delta S_{\ell m}^{T}\cos m\lambda)P_{\ell m}(\sin\varphi) \tag{17}$$

Temporal variations of surface deformation in east, north and up components (Zhang et al., 2017);

$$\Delta e_{(r,\varphi,\lambda)} = \frac{3a\times\rho_{w}}{\rho_{ave}\cos\varphi}\sum_{\ell=0}^{\ell_{\max}}\sum_{m=0}^{\ell}mP_{\ell m}(\sin\varphi)\frac{l_{\ell}}{2\ell+1}(-\Delta C_{\ell m}^{\sigma}\sin m\lambda + \Delta S_{\ell m}^{\sigma}\cos m\lambda) \tag{18}$$

$$\Delta n_{(r,\varphi,\lambda)} = -\frac{3a\rho_{w}}{\rho_{ave}}\sum_{\ell=0}^{\ell_{\max}}\sum_{m=0}^{\ell}m\frac{\partial P_{\ell m}(\sin\varphi)}{\partial\varphi}\frac{l_{\ell}}{2\ell+1}(\Delta C_{\ell m}^{\sigma}\cos m\lambda + m\Delta S_{\ell m}^{\sigma}\sin m\lambda) \tag{19}$$

$$\Delta h_{(r,\varphi,\lambda)} = \frac{3a\rho_{w}}{\rho_{ave}}\sum_{\ell=0}^{\ell_{\max}}\sum_{m=0}^{\ell}P_{\ell m}(\sin\varphi)\frac{h_{\ell}}{2\ell+1}(\Delta C_{\ell m}^{\sigma}\cos m\lambda + \Delta S_{\ell m}^{\sigma}\sin m\lambda) \tag{20}$$

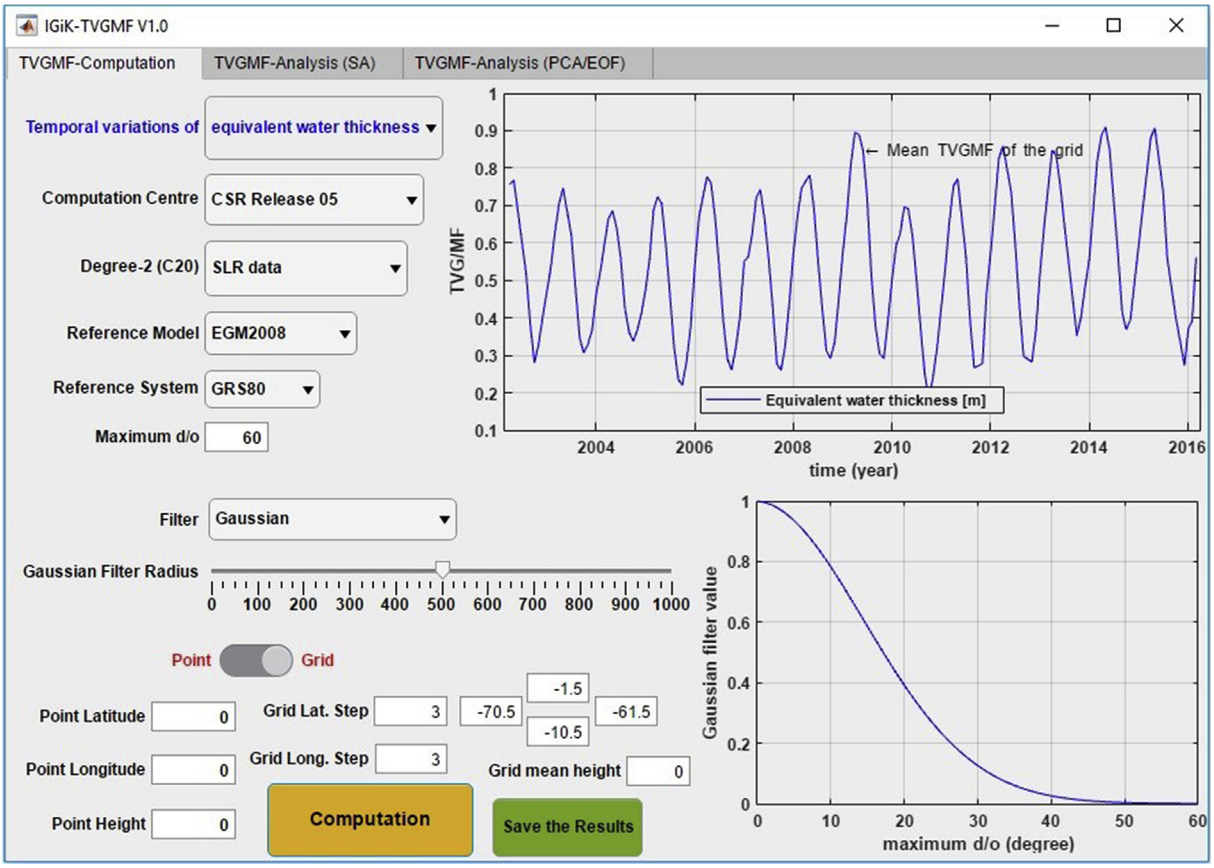

Fig. 3. Temporal variations of *EWT* at a grid of 3° × 3° spatial resolution and mean height of zero located in the Amazon basin (bounded by parallels of 1.5°S and 10.5°S and meridians of 61.5°W and 70.5°W) from the TVGMF–Computation.

With surface density coefficients $\Delta C^{\sigma}_{\ell m}$ and $\Delta S^{\sigma}_{\ell m}$ defined as

$$\begin{Bmatrix} \Delta C^{\sigma}_{\ell m} \\ \Delta S^{\sigma}_{\ell m} \end{Bmatrix} = \frac{\rho_{ave}}{3\rho_w} \frac{2\ell + 1}{1 + k_{\ell}} \begin{Bmatrix} \Delta C^{T}_{\ell m} \\ \Delta S^{T}_{\ell m} \end{Bmatrix} \tag{21}$$

where a is the radius of the Earth (semi-major axis), h, k and l denote the load Love numbers, ρ_{ave} and ρ_w are the average density of the Earth and the water density, respectively, and $\frac{\partial \bar{P}_{\ell m}(\sin\varphi)}{\partial\varphi}$ are the 1st derivative of the fully normalised Legendre functions with respect to φ that are determined using a recursive algorithm (Bosch, 2000; Appendix A). It should be noted that the 1st derivative of the fully normalised Legendre functions defined by other authors, e.g. Tscherning (1983), cannot be used at the poles (Bosch, 2000).

Assuming that temporal variations of ellipsoidal heights are represented by temporal variations of surface deformations in the up component, physical height (e.g. orthometric height) changes ΔH can be estimated using Eqs. (11) and (20) as follows (e.g. Godah et al., 2017b, 2017c):

$$\Delta H = \Delta h - \Delta N \tag{22}$$

It should be noted that Eq. (9)–(22) describe the computation of TVGMFs over a single point. However, when the computation of TVGMFs is performed over a grid, these equations will repeatedly be used to compute TVGMFs at each point of that grid.

3.3. Analysis and modelling of the TVGMF

Two methods, namely the seasonal adjustment (SA) method (Findley et al., 1998), also called seasonal decomposition method (e.g. Makridakis et al., 1998), and the Principal Component Analysis/Empirical Orthogonal Function (PCA/EOF) method (e.g. Jolliffe, 2002), were implemented in the IGiK–TVGMF to analyse and model the TVGMF. The fundamentals and the usefulness of these methods for the analysis and modelling of time series of the TVGMF were demonstrated by several authors (e.g. Rangelova, 2007; Forootan, 2014; Krynski et al., 2014; Godah et al., 2017a, 2018).

The main objective of the PCA/EOF is to reduce the dimensionality of the data vector and to identify the most important patterns explaining the variability within the data. It also aims at finding optimal orthogonal directions along which the observation values are maximally distributed. The PCA/EOF is considered among the most popular second order analysis techniques that have been used to extract dominant patterns from time series of geophysical data (e.g. Forootan, 2014). On the other hand, the main goal of the SA method is to decompose the time series signal into three components, i.e. Trend, Seasonal and Random components. Two models of the SA method (1) additive model (i.e. Trend + Seasonal + Random) and (2) Multiplicative model (i.e. Trend × Seasonal × Random) were defined (e.g. Makridakis et al., 1998). The additive model is suitable for time-series data of relatively constant seasonal variations. On the other hand, the multiplicative model is useful when the seasonal variation increases over time (ibid).

The SA method decomposes the TVGMF in the time domain, while the PCA/EOF method analyzes the TVGMF in the spatio-temporal domain. The main advantage of the PCA/EOF method compared to the SA method is that patterns in TVGMF can spatially be illustrated. The PCA/EOF method also superior the SA method for areas characterized with insignificant variation patterns of TVGMFs in the space domain (e.g. Godah et al., 2017a, 2018). On the other hand, the SA method performs slightly better than the PCA/EOF when there is a significant variation of TVGMF patterns in the space domain (see. Godah et al., 2017c).

The detailed algorithms and steps concerning the implementation of the SA method and the PCA/EOF method for the analysis and the

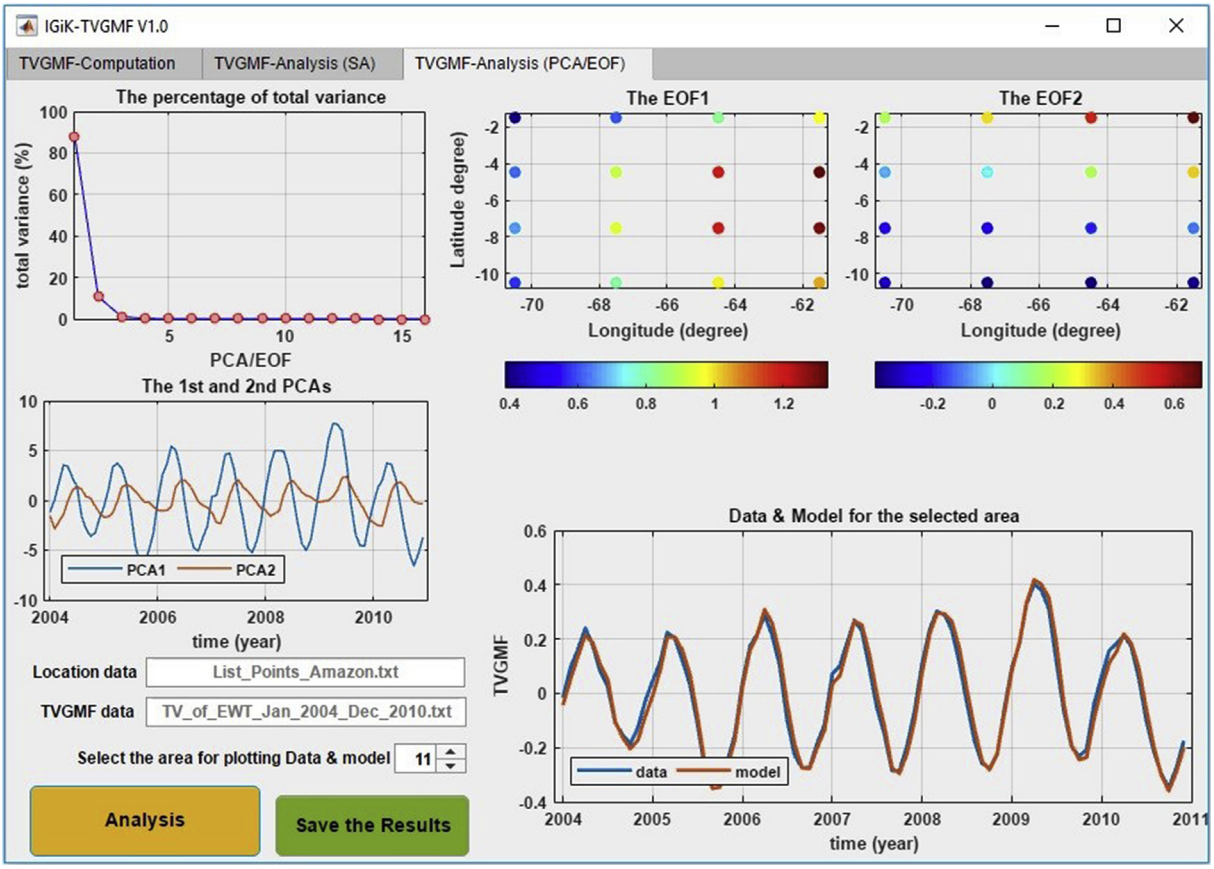

Fig. 4. Analysis of temporal variations of *EWT* at the Amazon basin (bounded by parallels of 1.5°S and 10.5°S and meridians of 61.5°W and 70.5°W) for the period between January 2004 and December 2010 using the TVGMF–Analysis (PCA/EOF).

modelling of TVGMFs were given in Godah et al. (2017a, 2018). However, in this section, these methods are described as far as they are relevant to the IGiK–TVGMF.

The seasonal variations of gravity/mass functionals are induced from the mass transport and mass distribution within the Earth system. In regional and global scales, amplitudes of such seasonal variations do not significantly increase over a couple of decades (e.g. Ilk et al., 2004; Jin, 2013). Thus, TVGMFs can be linked additively, and the additive model of the SA method can be applied. The TVGMF is decomposed into

$$\mathrm{TVGMF} = LT + S + E \tag{23}$$

where S denotes a seasonal component, LT is a long term/trend component and E is an unmodelled component.

The periodicities in TVGMF time series were estimated using periodogram values P that are computed as follows (see Eq. (13.1.4) in Wei, 2006; p. 290):

$$P_i = (a_i^2 + b_i^2)\frac{q}{2} \tag{24}$$

where a and b are Fourier coefficients, i denotes the month and q is the number of elements in the time series investigated.

The $\mathrm{TVGMF}^{\mathrm{model(SA)}}$ model in the SA method is developed as the sum of seasonal and long term/trend components

$$\mathrm{TVGMF}^{\mathrm{model(SA)}} = LT + S. \tag{25}$$

In the PCA/EOF method, TVGMF_i time series for points of the grid is constructed to the matrix $\mathbf{U}$. This matrix can be represented by the product of two matrices $\mathbf{V}$ and $\mathbf{P}$,

$$\mathbf{U} = \mathbf{V}\mathbf{P}^{\mathrm{T}} + \boldsymbol{\varepsilon} \tag{26}$$

where $\mathbf{V}$ consists of principal component analysis (PCA) modes, $\mathbf{P}$ is the loading matrix that defines the EOF loading patterns and reflects contributions of original variables to various PCA modes, and the matrix $\boldsymbol{\varepsilon}$ are unmodelled parts of TVGMF.

The PCA/EOF method relies on finding matrices $\mathbf{P}$ and $\mathbf{V}$. In the IGiK–TVGMF, these matrices were estimated using the SVD (Singular Value Decomposition) algorithm. The fraction of the total variance of TVGMF reflected by the PCA mode j was estimated as follows:

$$\sigma_j = \frac{\lambda_j}{\Delta},\ (j = 1,2,3,\ldots,t) \tag{27}$$

where λ_j denotes the eigenvalue estimated from TVGMF, t is the number of points of the grid and variable Δ is the total variance of TVGMF.

The $\mathrm{TVGMF}^{\mathrm{model(PCA/EOF)}}$ models developed with the use of the PCA/EOF method were obtained as

$$\mathrm{TVGMF}^{\mathrm{model(PCA/EOF)}} = \sum_{s=1}^{t} \mathrm{PCA}_s \cdot \mathrm{EOF}_s \tag{28}$$

4. Overview of the IGiK–TVGMF

The IGiK–TVGMF comprises of three graphical user interfaces (GUIs) developed with the use of a MATLAB R2017a App Designer (cf. https://www.mathworks.com/products/matlab/app-designer.html). The first GUI, named the TVGMF–Computation (cf. Figs. 1 and 3), is the main interface of the IGiK–TVGMF. In this GUI, thirteen TVGMFs can be determined at an individual point or a set of points, i.e. a grid of points, using GRACE-based GGMs from seven different computation centres (cf. Table 1). Different parameters, e.g. the Degree-2 (C_{20}), the reference model, the reference system and the maximum d/o, can be specified in this GUI. Moreover, in the TVGMF–Computation,

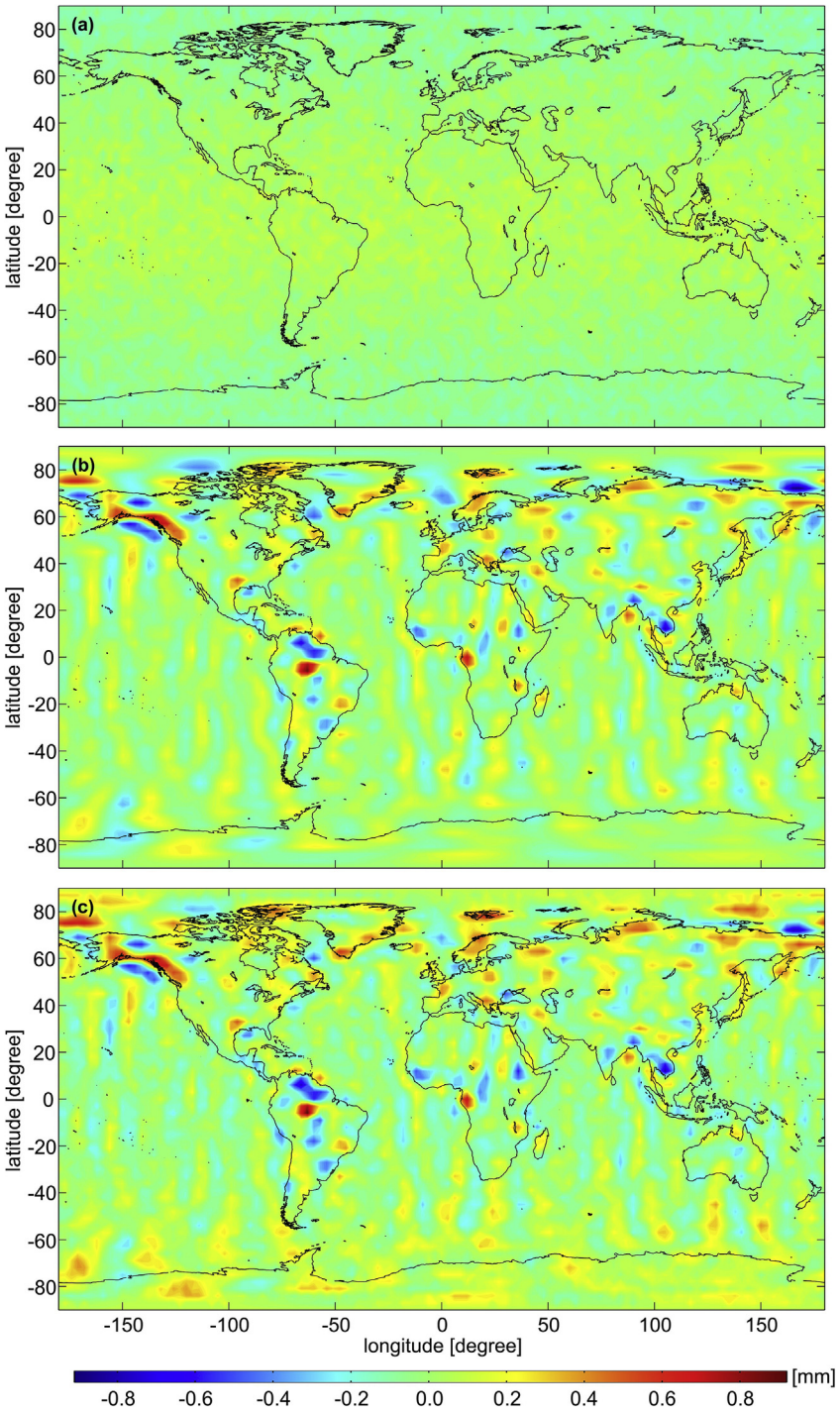

Fig. 5. The differences between ΔN obtained from (a) the IGiK–TVGMF and GRAVSOFT, i.e. ΔN_{IG-GR} (b) the IGiK–TVGMF and ICGEM CS, i.e. ΔN_{IG-IC}, and (c) the GRAVSOFT and ICGEM CS, i.e. ΔN_{GR-IC}.

Table 2
Statistics of ΔN_{IG-GR}, ΔN_{IG-IC} and ΔN_{GR-IC} (m).

	Min	Max	Mean	Std.
$\Delta N_{IG-GR} = \Delta N_{(IGiK-TVGMF)} - \Delta N_{(GRAVSOFT)}$	−0.00019	0.00014	–0.00002	0.00006
$\Delta N_{IG-IC} = \Delta N_{(IGiK-TVGMF)} - \Delta N_{(ICGEM\ CS)}$	−0.00091	0.00088	0.00000	0.00014
$\Delta N_{GR-IC} = \Delta N_{(GRAVSOFT)} - \Delta N_{(ICGEM\ CS)}$	−0.00084	0.00092	0.00002	0.00015

Table 3
The parameters applied in the TVGMF–Computation to validate TVGMFs.

TVGMF	Computation centres	Degree-2 (C_{20})	Reference Model	Reference System	Maximum d/o	Filter
Geoid heights	GFZ Release 05	SLR data	EIGEN-6C4	WGS84	60	DDK3
Equivalent water thickness	GFZ Release 05	SLR data	EIGEN-6C4	WGS84	60	DDK2
Gravity disturbance	GFZ Release 05	GRACE data	EGM2008	GRS80	90	DDK1
Gravity anomalies	GFZ Release 05	GRACE data	EGM2008	GRS80	90	DDK1
Deflections of the vertical (east–west component)	GFZ Release 05	GRACE data	GECO	GRS80	90	DDK1
Gravity gradients (the 2nd vertical derivative)	GFZ Release 05	GRACE data	GECO	GRS80	90	DDK1
Deflections of the vertical (north–south component)	GFZ Release 05	GRACE data	GECO	GRS80	90	DDK1

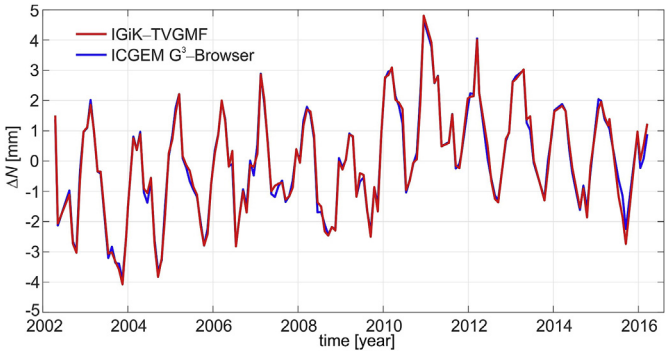

Fig. 6. Temporal variations of geoid heights ΔN at $\varphi = 53.5^{\circ}$ and $\lambda = 16.5^{\circ}$ from the IGiK–TVGMF (red line) and the ICGEM G^3-Browser (blue line). (For interpretation of the references to colour in this figure legend, the reader is referred to the Web version of this article.)

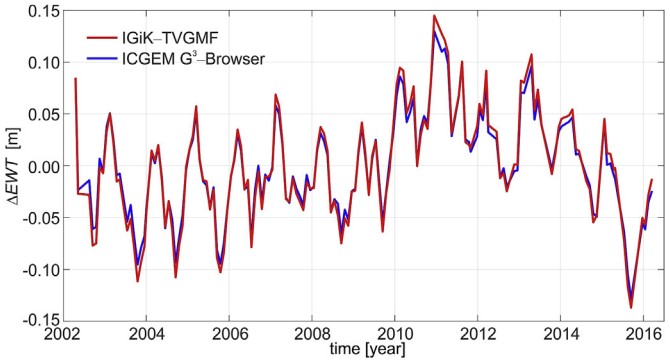

Fig. 7. Temporal variations of equivalent water thickness ΔEWT at $\varphi = 52.47^{\circ}$ and $\lambda = 21.03^{\circ}$ from the IGiK–TVGMF (red line) and the ICGEM G^3–Browser (blue line). (For interpretation of the references to colour in this figure legend, the reader is referred to the Web version of this article.)

decorrelation filters, i.e. DDK1, DDK2, …, and DDK8, (cf. Kusche et al., 2009), as well as the Gaussian filter of radius from 0 to 1000 km, can be applied to reduce noise, i.e. the north–south striped patterns, included in GRACE-based GGMs. The computed values of TVGMFs and the applied Gaussian filter can be visualized in panels of the TVGMF–Computation. The second and third GUIs, named the TVGMF–Analysis (PCA/EOF) and the TVGMF–Analysis (SA), respectively, were developed to analyse and model the TVGMF (cf. Figs. 2 and 4). In the current version of the IGiK–TVGMF, only data without gaps can be analysed using the SA and PCA/EOF methods. The components of TVGMF, the percentages of total variance, 1st and 2nd PCAs/EOFs and TVGMF data used in the analysis together with their model can be depicted in the panels of the TVGMF–Analysis (SA) and TVGMF–Analysis (PCA/EOF). In all those GUIs, numerical results with their metadata obtained from the computation or from the analysis can be saved as text files in an arbitrary folder specified by the user. The IGiK–TVGMF is optimized and tested on Microsoft Windows operating system. However, it might also be operated on Mac and Linux/Unix's operation systems.

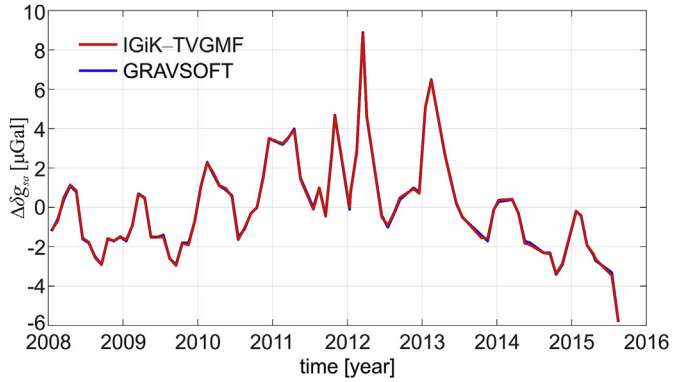

Fig. 8. Temporal variations of gravity disturbance $\Delta\delta g_{sa}$ at $\varphi = 52.47^{\circ}$ and $\lambda = 21.03^{\circ}$ from the IGiK–TVGMF (red line) and the GRAVSOFT package (blue line). (For interpretation of the references to colour in this figure legend, the reader is referred to the Web version of this article.)

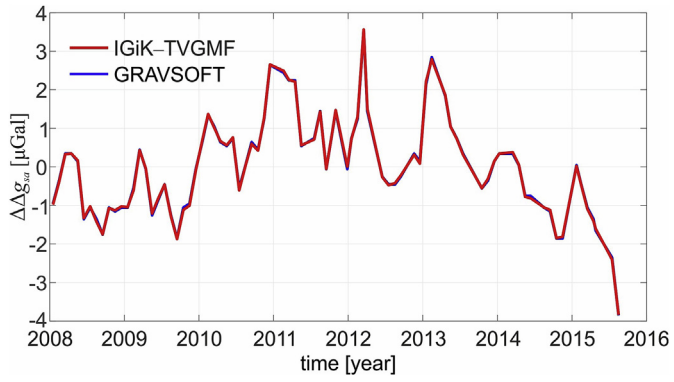

Fig. 9. Temporal variations of gravity anomalies $\Delta\Delta g_{sa}$ at $\varphi = 52.47^{\circ}$ and $\lambda = 21.03^{\circ}$ from the IGiK–TVGMF (red line) and the GRAVSOFT package (blue line). (For interpretation of the references to colour in this figure legend, the reader is referred to the Web version of this article.)

4. Examples of results of the IGiK–TVGMF

The implementation of the IGiK–TVGMF is exemplarily demonstrated. Two case studies were considered. They are conducted using a desktop computer equipped with an AMD FX (tm)-8350 Eight-Core processor and 16 GB of RAM (Random Access Memory). In the first case study, temporal variations of geoid heights at point P ($\varphi = 52^{\circ}$N, $\lambda = 20^{\circ}$E, $h = 0$) were determined and analysed. The parameters: **(a)** Computation Centre "GFZ Release 05", **(b)** Degree-2 (C_{20}) "SLR data", **(c)** Reference Model "EGM2008", **(d)** Reference System "GRS80", **(e)** Maximum d/o "60" and **(f)** Filter "Decorrelation (DDK3)", were chosen in the TVGMF–Computation (Fig. 1). The resulting time series of geoid heights variations are depicted in the upper-right panel in Fig. 1. Since the decorrelation filter is used, Gaussian filter coefficient values illustrated in the lower-right panel in Fig. 1 appear as a horizontal line of constant values equal to one. This computation indicates that the

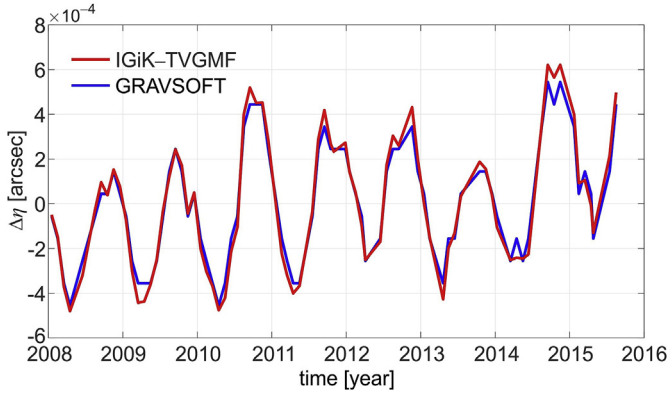

Fig. 10. Temporal variations of deflections of the vertical (east–west component) $\Delta\eta$ at $\varphi = 52.47^\circ$ and $\lambda = 21.03^\circ$ from the IGiK–TVGMF (red line) and the GRAVSOFT package (blue line). (For interpretation of the references to colour in this figure legend, the reader is referred to the Web version of this article.)

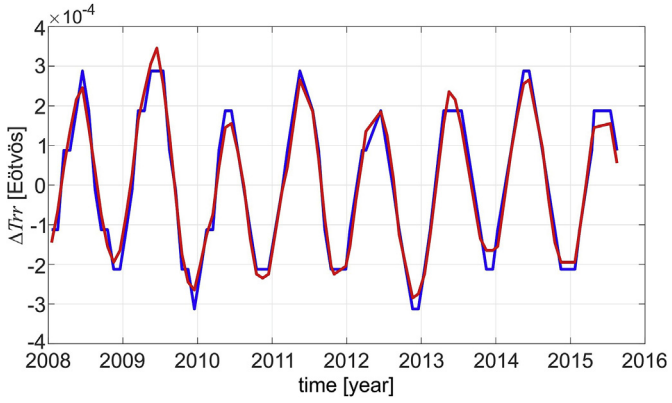

Fig. 11. Temporal variations of gravity gradients (the 2nd vertical derivative) ΔT_{rr} at $\varphi = 2.163^\circ$S and $\lambda = 55.126^\circ$W from the IGiK–TVGMF (red line) and the GRAVSOFT package (blue line). (For interpretation of the references to colour in this figure legend, the reader is referred to the Web version of this article.)

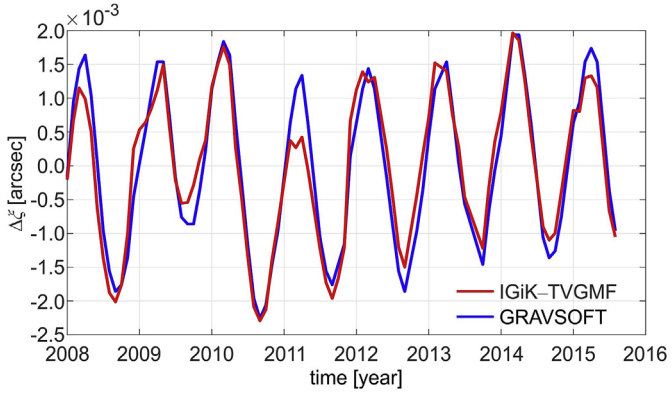

Fig. 12. Temporal variations of deflections of the vertical (north–south component) $\Delta\xi$ at the $\varphi = 2.163^\circ$S and $\lambda = 55.126^\circ$W from the IGiK–TVGMF (red line) and the GRAVSOFT package (blue line). (For interpretation of the references to colour in this figure legend, the reader is referred to the Web version of this article.)

elapsed time to compute TVGMFs at a single point using the TVGMF–Computation is ca. 32 s.

The determined temporal variations of geoid heights were analysed using the TVGMF–Analysis (SA). It should be noted that RL05 GRACE-based GGMs from the official GRACE Science Data System, i.e. CSR, GFZ and JPL, without gaps are available for the period from January 2004 to December 2010; for the remaining period, some gaps occur. Thus, temporal variations of geoid heights, for the period between January 2004 and December 2010, obtained at point *P*, were chosen for the analysis. Fig. 2 depicts the outcomes of the analysis. It consists of four panels that shows components of temporal variation of geoid heights, i.e. seasonal, long term/trend and unmodelled components, as well as temporal variations of geoid heights data and their model.

In the second case study, a grid of 3° × 3° spatial resolution and mean height of zero located in the Amazon basin, bounded by parallels of 1.5°S and 10.5°S and meridians of 61.5°W and 70.5°W, is considered. The temporal variations of *EWT* for this grid were determined using the TVGMF–Computation and the parameters: **(a)** Computation Centre "CSR Release 05", **(b)** Degree-2 (C_{20}) "GRACE data", **(c)** Reference Model "GECO", **(d)** Reference System "WGS84", **(e)** Maximum d/o "60", **(f)** Filter "Gaussian" and **(g)** Gaussian Filter Radius "500 km" (Fig. 3). Fig. 3 shows mean values of ΔEWT over the grid and the plot of Gaussian filter values coefficient. Moreover, the resulting temporal variations of *EWT*, for the period between January 2004 and December 2010, were analysed using the TVGMF–Analysis (PCA/EOF). Fig. 4 illustrates percentages of total variance of temporal variations of *EWT*, the first and second PCAs and EOFs. It also shows temporal variations of *EWT* data and their model for the point with ID number of eleven.

4.1. Examples of the validation of TVGMFs determined with use of the IGiK–TVGMF

Firstly, a comparison between TVGMFs from the IGiK–TVGMF, GRAVSOFT and ICGEM CS (ICGEM Calculation Service; http://icgem.gfz-potsdam.de/calc) has been conducted. As an example, geoid heights for March 2005 and September 2005 are determined at a global grid of 3° × 3° spatial resolution using GFZ GRACE-based GGMs truncated at d/o 60, the DDK3 filter, C_{20} from GRACE data, GRS80 and these three softwares. The differences between resulting geoid heights are obtained as follows:

$$\Delta N_{(\text{IGiK–TVGMF})} = N_{\text{IGiK–TVGMF (Mar. 2005)}} - N_{\text{IGiK–TVGMF (Sep. 2005)}} \quad (29)$$

$$\Delta N_{(\text{GRAVSOFT})} = N_{\text{GRAVSOFT (Mar. 2005)}} - N_{\text{GRAVSOFT (Sep. 2005)}} \quad (30)$$

$$\Delta N_{(\text{ICGEM CS})} = N_{\text{ICGEM CS (Mar. 2005)}} - N_{\text{ICGEM CS (Sep. 2005)}} \quad (31)$$

The differences $\Delta N_{\text{IG–GR}} = \Delta N_{(\text{IGiK–TVGMF})} - \Delta N_{(\text{GRAVSOFT})}$, $\Delta N_{\text{IG–IC}} = \Delta N_{(\text{IGiK–TVGMF})} - \Delta N_{(\text{ICGEM CS})}$ and $\Delta N_{\text{GR–IC}} = \Delta N_{(\text{GRAVSOFT})} - \Delta N_{(\text{ICGEM CS})}$ are obtained and depicted in Fig. 5. The statistics of these differences are given in Table 2.

The results presented in Fig. 5 and Table 2 reveal that the differences, in terms of maximum and minimum values, between ΔN obtained from the IGiK–TVGMF, GRAVSOFT and ICGEM CS are at the level of sub-millimetre. They also indicate that mean values and standard deviations of the differences between ΔN obtained from these three softwares are at the level 0.02 mm and 0.1 mm, respectively. Fig. 5 exhibits vertical stripes when comparing ΔN obtained from IGiK–TVGMF and from GRAVSOFT with the corresponding ones obtained from ICGEM CS. The main reason for these stripes might be ascribed to the fact that in the ICGEM CS, low pass filtering of gravity field models by gently cutting the spherical harmonic coefficients (cf. ftp://ftp.gfz-potsdam.de/home/sf/bar/OldPublications/gentlecut_engl.pdf) is compulsory applied. Overall, the results presented in Fig. 5 and Table 2 emphasize that ΔN from IGiK–TVGMF are conformable to the corresponding ones from the GRAVSOFT.

Secondly, seven time series of TVGMFs from the IGiK–TVGMF were validated with the corresponding ones from the GRAVSOFT package (Tscherning et al., 1992) and the ICGEM G^3–Browser (Barthelmes, 2016). Table 3 summaries the parameters applied in the TVGMF–Computation to determine these TVGMFs. Temporal variations of geoid heights are obtained at $\varphi = 53.5^\circ$ and $\lambda = 16.5^\circ$ (cf. Godah et al., 2017b), while temporal variations of gravity gradients (the 2nd

Table 4
Statistics of the differences between TVGMF from the IGiK–TVGMF and the corresponding ones from the GRAVSOFT or ICGEM G^3–Browser (cf. Fig. 6–12).

TVGMF		Unit	Min	Max	Mean	Std.
IGiK–TVGMF vs. ICGEM G^3–Browser	ΔN	m	-0.0005	0.0007	-5×10^{-18}	0.0002
	ΔEWT	m	-0.0172	0.0162	-8×10^{-17}	0.0070
IGiK–TVGMF vs. GRAVSOFT	Δg	mGal	-1×10^{-04}	1×10^{-04}	-7×10^{-17}	6×10^{-05}
	Δg_{sa}	mGal	-7×10^{-05}	7×10^{-05}	-4×10^{-16}	3×10^{-05}
	$\Delta\eta$	arcsec	-9×10^{-05}	1×10^{-04}	-3×10^{-16}	4×10^{-05}
	$\Delta\xi$	arcsec	-9×10^{-04}	7×10^{-04}	-5×10^{-17}	3×10^{-04}
	ΔT_{rr}	Eötvös	-5×10^{-05}	4×10^{-05}	-1×10^{-16}	3×10^{-05}

vertical derivative) and temporal variations of deflections of the vertical (north–south component) were determined at $\varphi = 2.163^{\circ}$S and $\lambda = 55.126^{\circ}$W. The remaining TVGMFs validated (see Table 3) were obtained at $\varphi = 52.47^{\circ}$ and $\lambda = 21.03^{\circ}$ (cf. Godah et al., 2016). It should be noted that, in Table 3, the parameters utilized to validate temporal variations of gravity gradients (the 2nd vertical derivative) and temporal variations of deflections of the vertical (north–south component) were arbitrary chosen. For the remaining TVGMFs, the selection of these parameters was based on previous investigations conducted in Godah et al. (2016; 2017a; 2017b; 2018). The results of the validation are shown in Figs. 6–12. The statistics of the differences between TVGMFs from the IGiK–TVGMF and the corresponding ones from the GRAVSOFT or from the ICGEM G^3–Browser are summarized in Table 4.

The results presented in Figs. 6 and 7 and Table 4 exhibit a very good agreement between the IGiK–TVGMF and the ICGEM G^3–Browser. They reveal that standard deviations of the differences between TVGMFs from IGiK–TVGMF and the respective ones from the ICGEM G^3–Browser are at the level of sub-millimetre for the geoid height and sub-centimetre for the equivalent water thickness. They also indicate that the differences, in terms of maximum and minimum values, can reach 0.7 mm and -1.7 cm for the geoid height and the equivalent water thickness, respectively. The reason for these differences might be due to the effect of the aforementioned guntelcut filter applied in the ICGEM solutions. Figs. 8–11 and Table 4 reveal that the differences between the corresponding Δg_{sa}, Δg, ΔT_{rr} and $\Delta\eta$ from the IGiK–TVGMF and the GRAVSOFT are within or beneath numerical values that can be provided by the GRAVSOFT, i.e. 1×10^{-4} or 4–decimals. Thus, these differences can be considered negligible. For some months, e.g. March 2011, slightly large, e.g. -9×10^{-4}, differences between $\Delta\xi$ obtained from the IGiK–TVGMF and the corresponding ones from the GRAVSOFT were observed (see Fig. 12). This might be due to the fact that $\frac{\partial P_{\ell m}(\sin\varphi)}{\partial\varphi}$ used in the IGiK–TVGMF are based on the Bosch (2000) while $\frac{\partial P_{\ell m}(\sin\varphi)}{\partial\varphi}$ used in the GRAVSOFT are based on the derivation given in Tscherning et al. (1983). However, Fig. 12 and Table 4 reveal that seasonal and the trend patterns in $\Delta\xi$ obtained from the IGiK–TVGMF and the corresponding ones from the GRAVSOFT do not change significantly and standard deviations of the differences between $\Delta\xi$ obtained from these softwares do not exceed 3×10^{-4} arcsec. Overall, they indicate that to some extend $\Delta\xi$ obtained from the IGiK–TVGMF agree with the corresponding ones obtained from the GRAVSOFT.

5. Conclusions and future developments

In this contribution, the IGiK–TVGMF, which is a new MATLAB package, for the determination and the analysis of temporal variations of gravity and mass functionals using GRACE-based GGMs is presented. It handles all available monthly GRACE-based GGMs from seven computational centres. The IGiK–TVGMF can be easily updated by including new GGMs developed from GRACE/GRACE-FO mission data and new degree-2 (C_{20}) data estimated from satellite laser ranging and ocean bottom pressure data. The differences between temporal variations of gravity/mass functionals from the IGiK–TVGMF and the corresponding ones from the GRAVSOFT package, the ICGEM CS and the ICGEM G^3–Browser are merely negligible. Overall, the IGiK–TVGMF overcomes some of the limitations of currently available softwares and interactive online tools developed for the computation and the analysis of TVGMFs. However, since the IGiK–TVGMF has been developed using MATLAB scripting language, it may perform slower compared to other softwares developed using high-level languages, e.g. FORTRAN, that can be compiled into the machine language and interactive online tools developed using the hypertext markup language. Thus, further improvements concerning the performance of the IGiK–TVGMF would be needed in the future research.

The IGiK–TVGMF is available as an open source that can be redistributed and/or modified under the terms of the GNU Library General Public License 3. Currently, the IGiK–TVGMF, including MATLAB functions and input datasets, is available at: https://github.com/Walyeldeen/Walyeldeen-Godah. The near future plan is to make it available via other sustained repository such as the repository of the Institute of Geodesy and Cartography (IGiK), Warsaw, Poland (http://www.igik.edu.pl/) and the European Observation System-Poland (EPOS-PL; https://epos-pl.eu/).

Acknowledgements

The research was conducted in the framework of the European Observation System-Poland (EPOS-PL), co-financed by the European Union from the European Regional Development Fund (POIR.04.02.00-14-A003/16-00). The GRACE-based GGMs included in the IGiK–TVGMF are acquired from the ICGEM. The author is thankful to Prof. J. Krynski and Dr. M. Szelachowska from the IGiK for their fruitful discussions and suggestions to develop the IGiK–TVGMF.

Appendix B. Supplementary data

Supplementary data to this article can be found online at https://doi.org/10.1016/j.cageo.2018.11.008.

Appendix A

The normalised associated Legendre functions $P_{\ell m}(\sin\varphi)$, up to d/o 120, are obtained as follows (e.g. Borre, 2008):

$$\left.\begin{aligned} P_{00}(\sin\varphi) &= 1.0 \\ P_{11}(\sin\varphi) &= \sqrt{3}\cos\varphi \\ P_{\ell,\ell}(\sin\varphi) &= \sqrt{\frac{2\ell+1}{\ell}}\cos\varphi P_{\ell-1,\ell-1}(\sin\varphi) \\ P_{\ell m}(\sin\varphi) &= \sqrt{\frac{(2\ell-1)(2\ell+1)}{(\ell-m)(\ell+m)}}\cos\varphi P_{\ell-1,m}(\sin\varphi) \\ &\quad -\sqrt{\frac{(2\ell+1)(\ell+m-1)(\ell-m-1)}{(2\ell-3)(\ell+m)(\ell-m)}}\cos\varphi P_{\ell-2,m}(\sin\varphi) \end{aligned}\right\} \tag{A1}$$

The $\frac{\partial P_{\ell m}(\sin\varphi)}{\partial\varphi}$ are obtained as follows (Bosch, 2000):

$$\left.\begin{aligned} &\text{for } 1 < m < \ell \\ &\quad 2\frac{\partial P_{\ell m}}{\partial\varphi} = \sqrt{(\ell+m)(\ell-m+1)}P_{\ell,m-1} \\ &\qquad -\sqrt{(\ell+m+1)(\ell-m)}P_{\ell,m+1} \\ &\text{for } m = 0 \\ &\quad \frac{\partial P_{00}}{\partial\varphi} = 0 \\ &\quad \frac{\partial P_{\ell 0}}{\partial\varphi} = -\sqrt{\frac{\ell(\ell+1)}{2}}P_{\ell,1} \\ &\text{for } m = 1 \\ &\quad \frac{\partial P_{11}}{\partial\varphi} = P_{\ell,0} \\ &\quad 2\frac{\partial P_{\ell 1}}{\partial\varphi} = \sqrt{\ell(\ell+1)}P_{\ell,0} - \sqrt{(\ell-1)(\ell+2)}P_{\ell,2} \\ &\text{and for } m = \ell > 1 \\ &\quad \frac{\partial P_{\ell\ell}}{\partial\varphi} = \sqrt{\frac{\ell}{2}}\,P_{\ell,\ell-1} \end{aligned}\right\} \tag{A2}$$

References

Barthelmes, F., 2013. Definition of Functionals of the Geopotential and Their Calculation from Spherical Harmonic Models: Theory and Formulas Used by the Calculation Service of the International Centre for Global Earth Models (ICGEM). GFZ German Research Centre for Geosciences. Potsdam, Germany, pp. 32. http://icgem.gfz-potsdam.de.

Barthelmes, F., 2016. International centre for global earth models (ICGEM). In: Drewes, H., Kuglitsch, F., Adám, J., Rózsa, S. (Eds.), The Geodesists Handbook 2016. Journal of Geodesy. vol. 90. pp. 1177–1180 10.

Bettadpur, S., 2013. CSR GRACE Release-05 Data Products: Status & Assessments. American Geophysical Union, Fall Meeting 2013, abstract #G33B-1004.

Borre, K., 2008. Geoid Undulations Computed from EGM96. Aalborg University. http://kom.aau.dk/~borre/masters/geoid/lecture2/geoidund.pdf.

Bosch, W., 2000. On the computation of derivatives of Legendre functions. Phys. Chem. Earth Solid Earth Geodes. 25 (9–11), 655–659. https://doi.org/10.1016/S1464-1895(00)00101-0.

Bucha, B., Janák, J., 2013. A MATLAB-based graphical user interface program for computing functionals of the geopotential up to ultra-high degrees and orders. Comput. Geosci. 56, 186–196.

Chen, Q., Shen, Y., Zhang, X., Hsu, H., Chen, W., Ju, X., Lou, L., 2015. Monthly gravity field models derived from GRACE Level 1B data using a modified short-arc approach. J. Geophys. Res.: Solid Earth 120 (3), 1804–1819.

Cheng, M.K., Tapley, B.D., Ries, J.C., 2013. Deceleration in the Earth's oblateness. J. Geophys. Res. 118, 1–8.

Dahle, C., Flechtner, F., Gruber, C., König, D., König, R., Michalak, G., Neumayer, K.H., 2014. GFZ RL05: an improved time-series of monthly GRACE gravity field solutions, observation of the system earth from space – CHAMP, GRACE, GOCE and future missions. Advanced Technologies in Earth Sciences 29–39.

Darbeheshti, N., Zhou, L., Tregoning, P., McClusky, S., Purcell, A., 2013. The ANU GRACE visualisation web portal. Comput. Geosci. 52, 227–233. https://doi.org/10.1016/j.cageo.2012.10.005.

Dziewonski, A.M., Anderson, D.L., 1981. Preliminary reference Earth model. Phys. Earth Planet. In. 25, 297–356. https://doi.org/10.1016/0031-9201(81)90046-7.

Findley, D.F., Monsell, B.C., Bell, W.R., Otto, M.C., Chen, B.-C., 1998. New capabilities and methods of the X-12-ARIMA seasonal-adjustment program. J. Bus. Econ. Stat. 16 (2), 127–152.

Forootan, E., 2014. Statistical Signal Decomposition Techniques for Analyzing Time-variable Satellite Gravimetry Data. PhD Thesis, vol. 131 University of Bonn. http://hss.ulb.uni-bonn.de/2014/3766/3766.htm.

Förste, C., Bruinsma, S.L., Abrikosov, O., Lemoine, J.-M., Marty, J.C., Flechtner, F., Balmino, G., Barthelmes, F., Biancale, R., 2014. EIGEN-6C4 the Latest Combined Global Gravity Field Model Including GOCE Data up to Degree and Order 2190 of GFZ Potsdam and GRGS Toulouse. GFZ Data Services. http://doi.org/10.5880/icgem.2015.1.

Gilardoni, M., Reguzzoni, M., Sampietro, D., 2016. GECO: a global gravity model by locally combining GOCE data and EGM2008. Studia Geophys. Geod. 60 (2), 228–247. https://doi.org/10.1007/s11200-015-1114-4.

Godah, W., Szelachowska, M., Krynski, J., 2017a. On the analysis of temporal geoid height variations obtained from GRACE-based GGMs over the area of Poland. Acta Geophysica 65 (4), 713–725.

Godah, W., Szelachowska, M., Krynski, J., 2017b. Investigation of geoid height variations and vertical displacements of the Earth surface in the context of the realization of the modern vertical reference system - a case study for Poland. International Association of Geodesy Symposia, Springer, Berlin, Heidelberg. https://doi.org/10.1007/1345_2017_15.

Godah, W., Szelachowska, M., Krynski, J., 2017c. On the estimation of physical height changes using GRACE satellite mission data – a case study of Central Europe. Geodesy Cartogr. 66 (2), 211–226. https://doi.org/10.1515/geocart-2017-0013.

Godah, W., Szelachowska, M., Krynski, J., 2018. Application of the PCA/EOF method for the analysis and modelling of temporal variations of geoid heights over Poland. Acta Geodaetica et Geophysica 53 (1), 93–105.

Godah, W., Szelachowska, M., Krynski, J., Dykowski, P., 2016. Analysis of RL05 GRACE-based and GOCE/GRACE-based GGMs Using Gravity Measurements at Borowa Gora Geodetic-geophysical Observatory. ESA special Publication SP-740.

Heiskanen, W.A., Moritz, H., 1967. Physical Geodesy. W.H. Freeman and Company, San Francisco.

Holmes, S.A., Pavlis, N.K., 2006. A FORTRAN program for very-high-degree harmonic synthesis. HARMONIC_SYNTH. http://earth-info.nga.mil/GandG/wgs84/gravitymod/new_egm/new_egm.html.

Ilk, K.-H., Flury, J., Rummel, R., Schwintzer, P., Bosch, W., Haas, C., Schröter, J., Stammer, D., Zahel, W., Miller, H., Dietrich, R., Huybrechts, R., Schmeling, H., Wolf, D., Riegger, J., Bardossy, A., Güntner, A., 2004. Mass transport and mass distribution in the earth system: contribution of the new generation of satellite gravity and altimetry missions to geosciences; proposal for a German priority research program, münchen: GOCE-projektbüro deutschland. Techn. Univ. München, GeoForschungsZentrum Potsdam, pp. 1–136.

Jin, S., 2013. Satellite Gravimetry: Mass Transport and Redistribution in the Earth System. Geodetic Sciences, IntechOpen, pp. 157–174. https://doi.org/10.5772/51698.

Jolliffe, I., 2002. Principal Component Analysis. Springer-Verlag, New York.

Kiamehr, R., Eshagh, M., 2008. EGMlab, a scientific software for determining the gravity and gradient components from global geopotential models. Earth Sci. India 1 (2), 93–103.

Klinger, B., Mayer-Gürr, T., Behzadpour, S., Ellmer, M., Kvas, A., Zehentner, N., 2016. The New ITSG-Grace2016 Release, vols. 17– 22 EGU General Assembly 2016, Vienna, Austria. https://doi.org/10.13140/RG.2.1.1856.7280. Apr. 2016.

Krynski, J., Kloch-Główka, G., Szelachowska, M., 2014. Analysis of time variations of the gravity field over Europe obtained from GRACE data in terms of geoid height and mass variations. In: In: Rizos, C., Willis, P. (Eds.), Earth on the Edge: Science for a Sustainable Planet. International Association of Geodesy Symposia, vol. 139. pp. 365–370. https://doi.org/10.1007/978-3-642-37222-3_48.

Kusche, J., Schmidt, R., Petrovic, S., Rietbroek, R., 2009. Decorrelated GRACE time-variable gravity solutions by GFZ, and their validation using a hydrological model. J. Geodes. 83 (10), 903–913.

Kusche, J., Schrama, E.J.O., 2005. Surface mass redistribution inversion from global GPS deformation and Gravity Recovery and Climate Experiment (GRACE) gravity data. J.

Geophys. Res. 110, B09409.
Makridakis, S., Wheelwright, S.C., Hyndman, R.J., 1998. Forecasting: Methods and Applications, third ed. Wiley, New York ISBN 978-0-471-53233-0.
Meyer, U., Jäggi, A., Jean, Y., Beutler, G., 2016. AIUB-RL02: an improved time-series of monthly gravity fields from GRACE data. Geophys. J. Int. 205 (2), 1196–1207. https://doi.org/10.1093/gji/ggw081.
Nielsen, J., Tscherning, C.C., Jansson, T.R.N., Forsberg, R., 2012. Development and user testing of a Python interface to the GRAVSOFT gravity field programs. In: In: Kenyon, S., Pacino, M., Marti, U. (Eds.), Geodesy for Planet Earth. International Association of Geodesy Symposia, vol. 136. pp. 443–449.
Pavlis, N.K., Holmes, S.A., Kenyon, S.C., Factor, J.K., 2012. The development and evaluation of the earth gravitational model 2008 (EGM2008). J. Geophys. Res. 117 (B04406), 1–38. https://doi.org/10.1029/2011JB008916.
Rangelova, E., 2007. A Dynamic Geoid Model for Canada. Ph.D. Thesis, University of Calgary, Department of Geomatics Engineering Report No. 20261.
Rapp, R.H., 1982. A Fortran Program for the Computation of Gravimetric Quantities from High Degree Spherical Harmonic Expansions. Report 334. Department of Geodetic Science and Surveying, The Ohio State University, Columbus.
Reigber, Ch, Lühr, H., Schwintzer, P., 2002. CHAMP mission status. Adv. Space Res. 30 (2), 129–134. https://doi.org/10.1016/S0273-1177(02)00276-4.
Sun, Y., Riva, R., Ditmar, P., 2016. Optimizing estimates of annual variations and trends in geocenter motion and J2 from a combination of GRACE data and geophysical models. J. Geophys. Res. 121 (11), 8352–8370. https://doi.org/10.1002/2016JB013073.
Tapley, B.D., Bettadpur, S., Watkins, M., Reigber, C., 2004. The gravity recovery and climate experiment: mission overview and early results. Geophys. Res. Lett. 31, L09607. https://doi.org/10.1029/2004GL019920.
Torge, W., Müller, J., 2012. Geodesy, fourth ed. Walter de Gruyter, Berlin-Boston.
Tscherning, C.C., Rapp, R.H., Goad, C., 1983. A comparison of methods for computing gravimetric quantities from high degree spherical harmonic expansions. Manuscripta Geod. 8, 249–272.
Tscherning, C.C., Forsberg, R., Knudsen, P., 1992. The GRAVSOFT package for geoid determination. Proceedings of the 1st Continental Workshop on the Geoisd in Europe. Research Institute of Geodesy, Topography and Cartography, Prague, pp. 327–334 Prague.
Wahr, J., Molenaar, M., Bryan, F., 1998. Time variability of the Earth's gravity field: hydrological and oceanic effects and their possible detection using GRACE. J. Geophys. Res. 103 (B12), 30205–30229.
Wang, H., Xiang, L., Jia, L., Jiang, L., Wang, Z., Hu, B., Gao, P., 2012. Load Love numbers and Green's functions for elastic Earth models PREM, iasp91, ak135, and modified models with refined crustal structure from Crust 2.0. Comput. Geosci. 49, 190–199. https://doi.org/10.1016/j.cageo.2012.06.022.
Watkins, M.M., Yuan, D.-N., 2014. GRACE: JPL Level-2 Processing Standards Document for Level-2 Product Release 05.1. Jet Propulsion Laboratory, California Institute of Technology, pp. 14 GRACE 327–744 v5.1.
Wei, W., 2006. Time Series Analysis: Univariate and Multivariate Methods, second ed. Pearson Addison Wesley, New York.
Weigelt, M., van Dam, T., Jäggi, A., Prange, L., Tourian, M.J., Keller, W., Sneeuw, N., 2013. Time-variable gravity signal in Greenland revealed by high-low satellite-to-satellite tracking. J. Geophys. Res.: Solid Earth 118, 3848–3859. https://doi.org/10.1002/jgrb.50283.
Zehentner, N., Mayer-Gürr, T., Weigelt, M., Jäggi, A., 2014. Non-dedicated satellite missions for time variable gravity field estimation. In: Grace Science Team Meeting, Potsdam, 28–30 Sept. 2014.
Zhang, X., Jin, S., Lu, X., 2017. Global surface mass variations from continuous GPS observations and satellite altimetry data. Rem. Sens. 9 (10), 1000. https://doi.org/10.3390/rs9101000.
Zhou, H., Luo, Z., Zhou, Z., Zhong, B., Hsu, H., 2017. HUST-Grace2016s: a new GRACE static gravity field model derived from a modified dynamic approach over a 13-year observation period. Adv. Space Res. 60 (3), 597–611. https://doi.org/10.1016/j.asr.2017.04.026.